PERGAMON

PII: S1359-6454(99)00008-7

Acta mater. Vol. 47, No. 4, pp. 1117–1128, 1999

Printed in Great Britain
1359-6454/99 $19.00 + 0.00

DIFFUSION-LIMITED REACTIVE WETTING: STUDY OF SPREADING KINETICS OF Cu–Cr ALLOYS ON CARBON SUBSTRATES

R. VOITOVITCH†[1], A. MORTENSEN[2], F. HODAJ[1] and N. EUSTATHOPOULOS[1]‡

[1]Institut National Polytechnique de Grenoble, ENSEEG, Laboratoire de Thermodynamique et Physico-Chimie Métallurgiques, URA 29, Domaine Universitaire, 38402 Saint Martin d'Hères cedex, France and [2]Department of Materials, Swiss Federal Institute of Technology in Lausanne (EPFL), CH-1015 Lausanne, Switzerland

(Received 17 July 1998; received in revised form 21 December 1998; accepted 3 January 1999)

Abstract—Spreading kinetics of Cu–Cr alloys diluted in Cr on smooth vitreous carbon substrates are studied by the "transferred drop" variant of the sessile drop technique under high vacuum. In this system, the transition from large, non-wetting, contact angles to low-wetting contact angles is due to the formation of a continuous layer of wettable chromium carbide along the liquid–solid interface. It is shown that the drop spreading rate is controlled by diffusion of the reactive atom species (Cr) from the bulk liquid to the solid–liquid–vapor triple line. Results for the dependence of spreading rate on time, drop mass, and alloy composition are compared with the predictions of a recently published model for diffusion-limited reactive wetting. © *1999 Acta Metallurgica Inc. Published by Elsevier Science Ltd. All rights reserved.*

1. INTRODUCTION

Recent sessile drop experiments on metal–ceramic systems [1, 2] have shown that a sufficient condition for improving wetting of a given substrate by a given metal is to alloy the metal with a chemical species which reacts with the substrate to form a dense layer of solid reaction product that is better wetted by the metal than the original substrate [3]. When such interfacial reactions drive wetting, it is observed that spreading of the drop on the substrate takes place at a far lower rate than is commonly observed in non-reactive wetting by liquid metals. Indeed, observed spreading times for small metal droplets lie, in reactive wetting, typically between 10 and 10 000 s, whereas in non-reactive systems, for which the rate of spreading is limited solely by viscous and inertial forces, small metallic drops spread in less than 0.1 s [4]. For this reason, it has been concluded that in reactive systems, spreading is not controlled by viscous or inertial forces, but rather by the rate of the interfacial reaction itself [5].

The rate of the interfacial reaction, in turn, may be controlled by the slower of two successive phenomena that intervene in the reaction process: local reaction kinetics at the triple line, and diffusive transport of reacting species to or from the triple line [5]. In the first limit, of control by local reaction kinetics, the rate of reaction and hence the triple line velocity are expected to be constant in time [5]. This is confirmed by experiment: constant triple line velocities have indeed been observed in the CuSi/C system [6], and also for unalloyed aluminum on carbon (for which diffusion clearly does not intervene) [5]; these two systems are thus representative of the first limit.

In the second limit, diffusion is rate-limiting: local reaction rates are comparatively rapid, and the extent of local reaction which drives spreading is limited by the diffusive supply of reactant from the drop bulk to the triple line. In contrast with the previous limiting case, the rate of isothermal spreading may then depend on time. Examples of time-dependent spreading rates are indeed found with CuPdTi on alumina and silica substrates [1] and with Cu–Ti on alumina [7]. Unfortunately, owing to the technique used and to the characteristics of CuPd–Ti and CuTi phase diagrams, these sessile drop spreading experiments were not isothermal, which complicates significantly interpretation of the spreading kinetics observed.

We therefore present in what follows experimental data gathered on another system, free of problems previously encountered. This system consists of vitreous carbon (C_v) substrates and copper drops containing small additions of chromium. Chromium reacts with carbon, forming at the interface a continous layer of chromium carbide which is comparatively well wetted by the alloy [8–10]. To obtain rigorously isothermal wetting conditions, sessile drop experiments were conducted using the "transferred drop" variant of the sessile drop technique,

†Now with the Institute for Materials Problems, Kiev, Ukraine.

‡To whom all correspondence should be addressed.

whereby wetting is initiated by rapid capillary contact of the drop with the solid substrate to be wetted. The advantage of this technique, as will be apparent below, is that wetting is initiated after the experimental system temperature has stabilized at a value above the droplet melting point.

2. EXPERIMENTAL PROCEDURE

Vitreous carbon (C_v) substrates having no open porosity, an ash content less than 50 ppm and, after polishing, an average surface roughness of 2 nm were employed. Before the experiments, all substrates were ultrasonically cleaned in acetone and then annealed. Copper–chromium alloy droplets were prepared from pure Cu (99.999%) and Cr (99.3%) during experiments by melting and alloying on flat horizontal substrates of pure monocrystalline alumina. Copper–chromium alloys do not wet alumina ($\theta > 90°$), and interfacial reactivity is negligible on such substrates [11].

Above the droplet and its alumina substrate, a flat vitreous carbon (C_v) substrate was placed about 5–10 mm from the top droplet surface, Fig. 1(a). Once the drop was molten and alloyed, and the chosen experiment temperature of 1373 K was attained and stable, the drop resting on its initial alumina substrate was raised so as to initiate contact of its upper surface with the C_v substrate. At that moment, capillary forces caused rapid isothermal spreading of the drop in contact with the carbon substrate to a first (metastable) equilibrium position, where the drop formed a pendular bridge between the two substrates [Fig. 1(b)]. Thereafter, the drop contact angle on the upper carbon substrate evolved with time: this evolution was monitored by continuous observation of the triple line position and contact angle along the upper carbon substrate. As spreading of the pendular drop over the carbon substrate progressed under the action of reaction-enhanced wetting, the liquid bridge between the two substrates became unstable at some point in time. At that moment, designated in what follows as t_1, most of the pendular drop suddenly detached from the lower alumina substrate, and from then on took the form of a sessile droplet hanging from the carbon substrate [Fig. 1(c)]. This hanging droplet then continued spreading over the carbon substrate, until final equilibrium was reached.

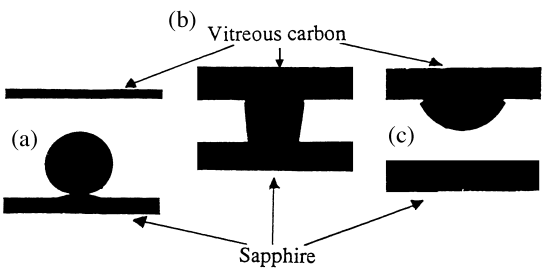

Fig. 1. Shadow pictures of drop configuration in a "transferred drop" wetting experiment of Cu–Cr alloy on vitreous carbon. (a) Initial configuration, (b) pendular drop configuration upon initial contact with the upper substrate, and (c) hanging drop after separation from the lower substrate, caused by gradual spreading on the upper substrate.

The experiments were performed in a high-vacuum metallic furnace under a dynamic vacuum of 10^{-3} Pa obtained by purified helium microleaks. This apparatus consisted essentially of a molybdenum resistance furnace fitted with windows enabling direct illumination of the sessile drop on the substrate. The spreading process was filmed by a video camera connected to a computer enabling automatic image analysis. After the experiments, the measured contact angle, θ, as well as the drop base radius, R, were computed directly from the recorded drop profile with an accuracy of $\pm 2°$ for θ and $\pm 2\%$ for R. After cooling the drop, the interfacial reaction product chemistry and morphology were characterized in selected specimens by scanning electron microscopy, electron probe microanalysis, and X-ray diffraction.

Such transferred drop experiments were performed with chromium concentrations ranging from 0.5 to 2 at.% on vitreous carbon. For comparison purposes, one additional experiment was performed using the same technique for a drop of Cu–40 at.% Si alloy, also on vitreous carbon. As mentioned above, it is known that reactive spreading occurs for this system with a constant triple line velocity (i.e. for this system, spreading kinetics are linear).

3. RESULTS

The main experimental parameters which were varied were the drop mass, between 35 and 350 mg, and the alloy Cr content, between 0.5 and 2 at.%. In all experiments, the final contact angle, θ_f, was found to be constant, equalling $41 \pm 4°$ irrespective of chromium concentration in the alloy or drop mass.

Figures 2(a) and (b) shows an example of variations with time of drop radius (R) and contact angle (θ) for two Cu–Cr drops having nearly the same mass and the same molar fraction of chromium. Results are identical except towards the end of spreading, the final contact angles being slightly different between the two drops (45° and 38°). This illustrates the overall good reproducibility obtained in the experiments.

Observed triple line velocities are clearly not constant in time. Up to $t = t_1$ (defined on the graph), the liquid is in contact with two substrates, alumina below the drop, and carbon above. At $t = t_1$, the drop is transferred to the carbon substrate, as described above. Thereafter, it takes the shape of a spherical cap. It is clearly seen that at $t = t_1$, the change of drop configuration accompanying separ-

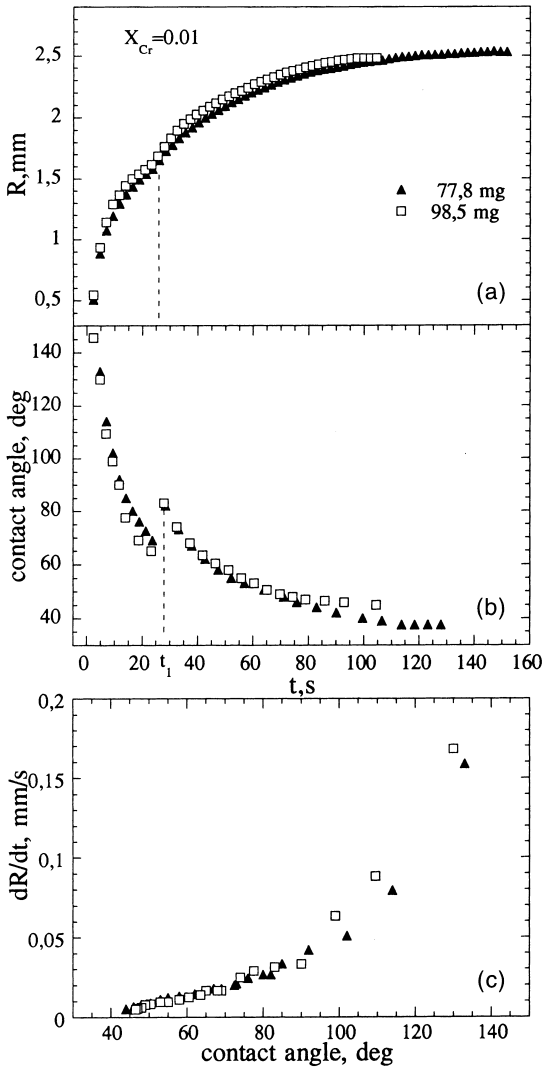

Fig. 2. Wetting kinetics of Cu–Cr alloys on the C_v substrates for two separate experiments, showing the reproducibility of the data.

ation from the lower substrate causes a significant increase in contact angle θ; at the same time, the triple line velocity strongly and discontinuously increases.

In Fig. 3 the drop base radius R as a function of time and the triple line velocity (dR/dt) as a function of instantaneous contact angle (θ) are plotted for three Cu–Cr alloys having different nominal contents of chromium: it is seen that the same discontinuity in triple line velocity is observed upon drop transfer as in Fig. 2, and that the triple line velocity increases with the nominal alloy Cr concentration.

After cooling of the samples, analysis of selected specimens showed the formation at the interface of a dense reaction layer having a thickness between 1 and 5 μm (Fig. 4). This thickness was uniform across the liquid–solid contact area for each drop; however, this thickness depended on drop Cr content and on the time of holding at 1373 K. Microprobe analysis of the thickest of these layers led to identification of the compound Cr_7C_3 rather than Cr_3C_2 found in previous studies [9, 10]. X-ray diffraction performed on the chromium carbide after elimination by chemical dissolution of the Cu–Cr alloy confirmed Cr_7C_3 formation.

The Cr content of the solidified drops was also measured by microprobe analysis. Because the microstructure of the solidified drops featured both primary copper dendrites and eutectic phases, the accuracy of these determinations was low; however, the results did show final Cr contents in the solidified droplet lower by a factor of two in comparison

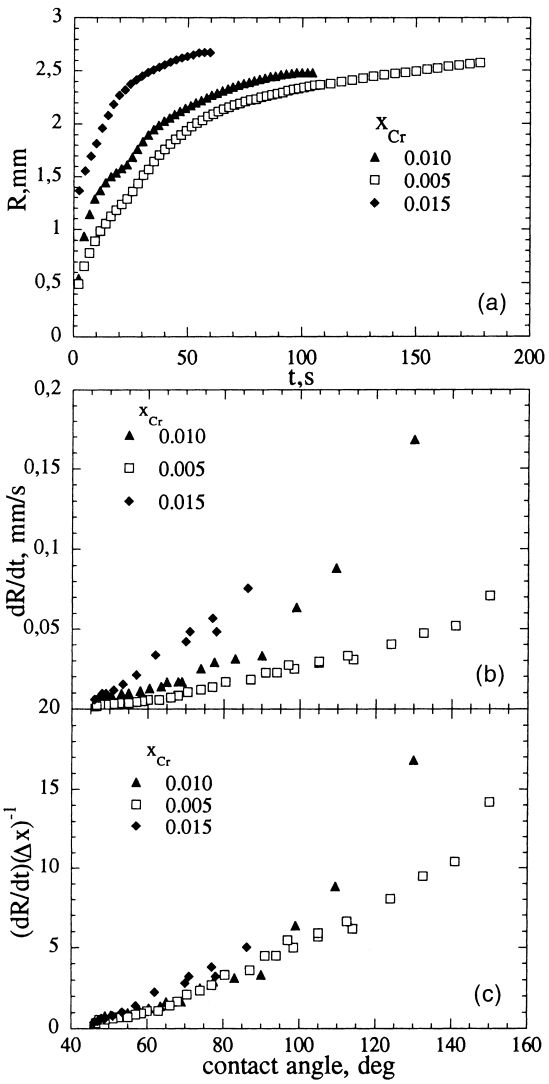

Fig. 3. Wetting kinetics of Cu–Cr alloys on vitreous carbon substrates, influence of nominal Cr content in the alloy: (a) drop radius R as a function of time, (b) triple line velocity dR/dt as a function of instantaneous contact angle θ, (c) as in (b) after normalization by solute concentration (see Discussion, Section 4).

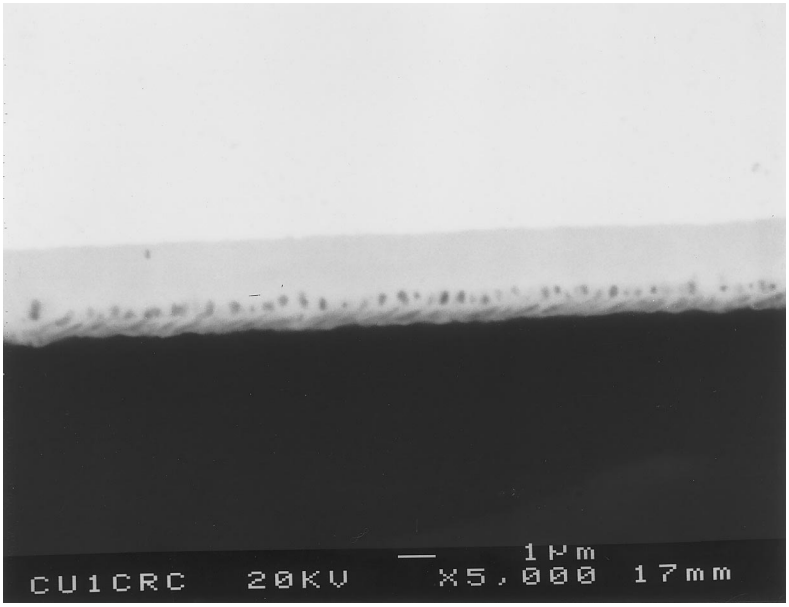

Fig. 4. Micrograph of drop–substrate interface for Cu–1 at.% Cr alloy on C_v (T = 1373 K, t = 5 min), showing chromium carbide formation.

with the nominal initial alloy concentration. This indicates that there is some loss of chromium from the drop during the experiment, which can be attributed to two phenomena: (i) evaporation, occuring mainly during the formation of the Cu–Cr alloy on the initial alumina substrate, i.e. before the onset of spreading on carbon substrates; and (ii) chromium carbide formation at the drop–carbon substrate interface.

Table 1 presents, for three selected experiments, the values of the nominal drop Cr content, x_{nom}, the final drop Cr content determined by microprobe analysis, $x_{f,exp}$, and corresponding final concentration values, $x_{f,cal}$, calculated by taking into account Cr losses due to evaporation (evaluated from drop mass losses) and to the interfacial reaction (evaluated by measuring along the interface the reaction layer thickness). Calculated and experimental values of x_f are in good agreement. In Table 1, two more values of Cr content are given: (i) x_{in}, the estimated initial drop composition at the beginning of the experiment, i.e. when the drop is first put into contact with the upper substrate, calculated assuming a constant evaporation rate; and (ii) x_{t1}, the estimated drop composition at $t = t_1$, i.e. immediately after drop transfer. This value was calculated by substraction of chromium eliminated by evaporation and reaction along the contact surface at $t = t_1$.

Table 1. Chromium molar fractions in Cu for three droplets: nominal value (x_{nom}), measured final value from microprobe analysis ($x_{f,exp}$), estimated values at the beginning of the experiment (x_{in}), at the end of the experiment ($x_{f,cal}$) and at $t = t_1$, i.e. immediately after drop transfer (x_{t_1})

x_{nom}	x_{in}	x_{t_1}	$x_{f,cal}$	$x_{f,exp}$
0.0053	0.0045	0.0036	0.0024	0.002
0.0101	0.0087	0.0071	0.0051	0.0045
0.0235	0.0230	0.0178	0.0153	0.012

Chromium losses by evaporation during the initial hold period preceding contact of the drop with the upper carbon substrate, raises the concern that small quantities of chromium carbide may have formed on the carbon substrate before contact of the drop, and influence spreading kinetics. It is clear from the data (see below) that the substrates were not covered with a continuous layer of chromium carbide Cr_7C_3—measured spreading rates are higher by two orders of magnitude than those that have been recorded for the same alloys spreading over a continuous layer of Cr_7C_3 [8]. Therefore, the only open question left was whether chromium evaporation from the drop onto the substrate before drop contact could cause the formation of isolated carbide islands on the carbon substrate. Selected experiments were therefore conducted several times, with all parameters constant except for the initial holding time: no acceleration with increasing holding time was observed for subsequent drop spreading kinetics. Thus, there is also no partial carbide formation on the substrate before drop spreading, since otherwise more rapid drop spreading would be observed after the longer holding time.

4. DISCUSSION

The addition of Cr to Cu clearly leads to a strong decrease of the final contact angle θ on vitreous car-

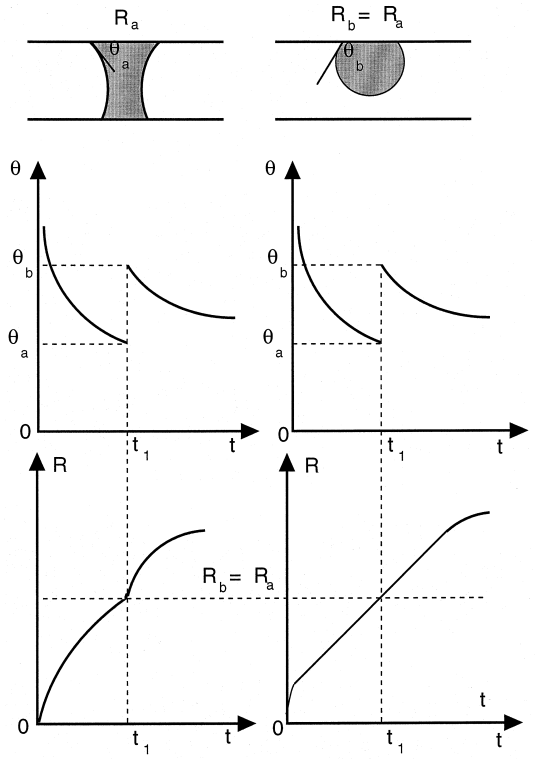

Fig. 5. Schematic description of the evolution of drop contact angle θ and contact radius R as a function of time in the vicinity of drop transfer ($t = t_1$), for (i) a system such as Cu–Cr on vitreous carbon for which spreading kinetics show a discontinuity in spreading rate upon drop transfer, indicating a dependence of spreading rate dR/dt on contact angle θ (a), and (ii) a system such as Cu–40 at.% Si on vitreous carbon, for which the spreading rate is constant and independent of contact angle θ over a large range of variation of this parameter. These functional dependences of spreading rate upon drop transfer are indicative of diffusion control, and local reaction control, of spreading kinetics, respectively.

bon, from 137° to about 40°. As was shown elsewhere, this last value is nearly equal to the contact angle of Cu–Cr alloy on a substrate of chromium carbide [8].

The continuous loss of chromium from the drop, both before and during the spreading process, introduces a complicating factor in the present data: by comparison of the estimated drop chromium content at the beginning of the spreading process, x_{in} in Table 1, with the final drop chromium content, x_f, it is seen that during spreading the chromium concentration decreases significantly; this could potentially cause the observed non-linear nature of spreading kinetics in this system.

This complicating factor is, however, circumvented by closer examination of the data at the moment of drop transfer, t_1. Indeed, at that moment, although the drop contact area with the upper substrate remains constant, the contact angle θ increases suddenly, from θ_a to θ_b, as a consequence of the sudden increase of the liquid volume supported by the upper substrate (clearly, θ_b is an "advancing" contact angle) while the drop bulk chromium content remains constant given the very short time of transfer [Figs 5(a) and (b)]. It can be seen, on the experimental plots of drop radius R or spreading rate dR/dt vs time (Figs 2 and 3) that this sudden increase in θ at t_1 produces a significant and discontinuous increase in the spreading rate for the present system, as depicted schematically in Fig. 5(c) on the left-hand side. The spreading rate depends therefore—for Cu–Cr on vitreous carbon—on the instantaneous geometry of the drop and hence on the contact angle θ.

For comparison, data are presented in Fig. 6 for a similar "transferred drop" experiment with Cu–40 at.% Si on vitreous carbon. For this system, it is known that the spreading rate is constant in a large range of θ, and governed by local reaction kinetics instead of solute diffusion to the triple line. It is seen that a plot of R vs time now yields a single straight line, as depicted schematically on the right-hand side of Fig. 5(c), such that the spreading rate, dR/dt, remains undisturbed by the drop transfer

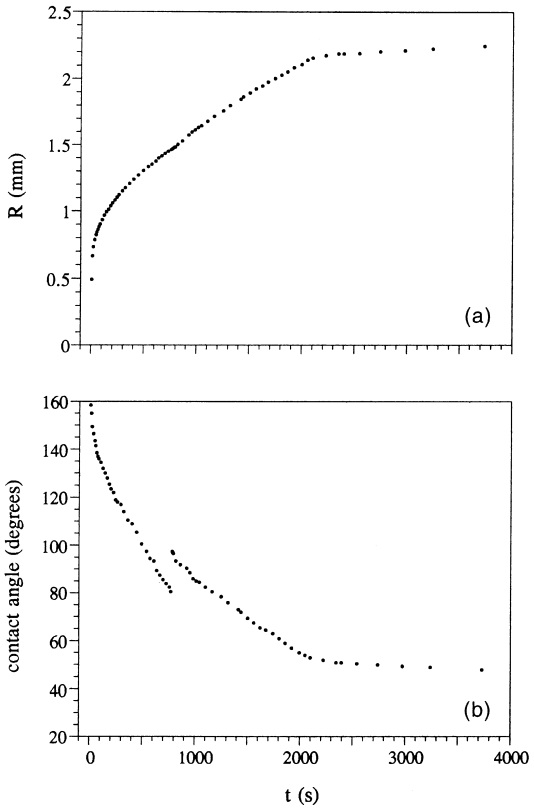

Fig. 6. Contact radius R and contact angle θ as a function of time for Cu–40 at.% Si on vitreous carbon at 1373 K ($m = 59.4$ mg). Note the lack of discontinuity in spreading rate (dR/dt) at the moment of drop transfer, $t = t_1$, in contrast with observations for Cu–Cr alloys on the same substrate (Fig. 2).

process despite the sudden increase in contact angle θ. This is as expected for a spreading process limited only by processes occurring at the triple line itself.

It can thus be concluded that in the Cu–Cr/C_v system, spreading kinetics are influenced significantly by the diffusion of chromium to the triple line. The role of diffusion can be examined more precisely by comparison of data with a recently proposed analytical model for the rate of triple line motion under bulk diffusion control [12]. This analysis is based on several assumptions, in particular that convection in the drop and reaction at the interface behind the triple line can both be neglected. Its principal conclusion is that, due to the essentially cylindrical nature of the diffusion problem at hand, the time dependence of the rate of solute diffusion to the triple line can be ignored as long as the solute-depleted region near the triple line does not extend as far as the center of the drop. As a consequence, the triple line velocity, dR/dt, varies with time only through its linear relation with the instantaneous contact angle θ:

$$\frac{dR}{dt} = \frac{2DF_{(t)}}{en_v}(C_0 - C_e)\theta \qquad (1)$$

where D is the diffusion coefficient in the liquid phase, n_v is the number of moles of reactive solute per unit volume of the reaction product, e is the reaction product thickness at the triple line, C_0 is the bulk drop concentration, C_e is the concentration of reactive solute in equilibrium with the reaction product (such that $C = C_e$ at the triple line), and $F_{(t)}$ is a function of time t which varies very little, and can thus be considered constant, with a value near 0.04 in usual sessile drop experiments [12]. For a spherical cap shaped droplet of volume V and for sufficiently low contact angles ($\theta < 60°$), the contact angle is closely approximated by $\theta = 4V/(\pi R^3)$; when introduced into equation (1), this yields $R^4 - R_0^4 = \text{const.} \times Vt$, where V is the drop volume.

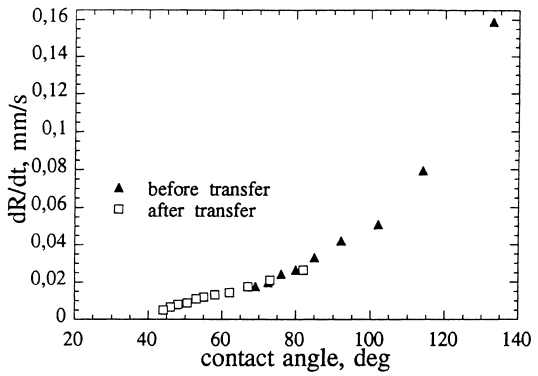

Fig. 7. Triple line velocity as a function of instantaneous contact angle θ before and after transfer of a 77.8 mg drop with a nominal Cr content $x_{Cr} = 0.01$, showing that the spreading rate depends directly on θ and not on time.

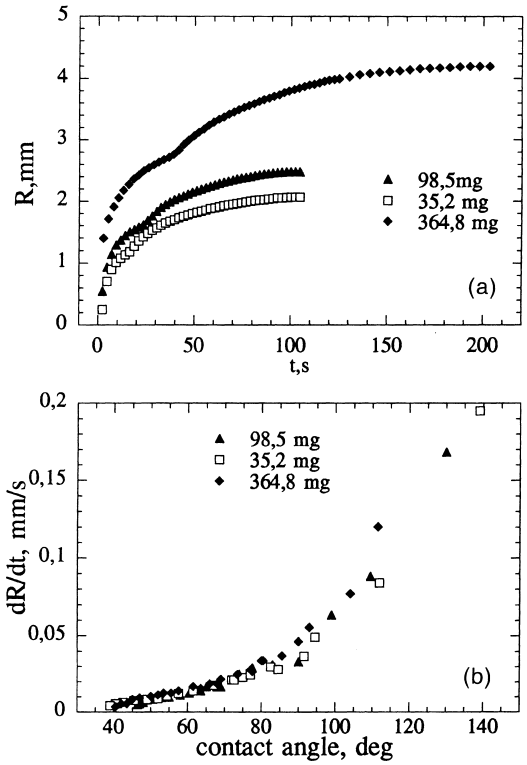

Fig. 8. Wetting kinetics of Cu–Cr alloys on vitreous carbon substrates. Influence of drop mass: (a) drop radius R as a function of time; (b) triple line velocity dR/dt as a function of instantaneous contact angle θ.

The experimental data agree with this analysis in several respects.

- The triple line velocity dR/dt is indeed, for all experiments, a time-independent function of the instantaneous contact angle θ. This is shown quite eloquently by the fact that for the same contact angle θ the corresponding triple line velocities before and after drop transfer are nearly equal (the influence of chromium depletion is negligible for the short times involved); see Fig. 7, where different symbols are used to mark the change in drop configuration. This direct dependence of dR/dt on θ before and after drop transfer is also visible in Figs 2(c) and 3(b), since the data retrace a portion of the same curve of dR/dt vs θ upon drop transfer.
- This direct dependence of spreading rate on the instantaneous contact angle θ is further confirmed in Fig. 8(a), which presents variations with time of drop base radius (R) as a function of time for three Cu–Cr drops having the same nominal chromium content (of 1 at.%), but varying mass. When these data are plotted in the form of triple line velocity dR/dt as a function of instantaneous contact angle θ [Fig. 8(b)], it is seen that the values of the contact line velocity belong to the same curve irrespective of drop mass. The data thus confirm clearly the principal conclusion of

Ref. [12], namely that time does not *per se* appear to be an important parameter despite the transient nature of the governing diffusion process. As a consequence, the spreading rate is a direct function of the instantaneous contact angle θ. As discussed in Ref. [12], this is due to the essentially cylindrical nature of the diffusion problem at hand.

- The triple line velocity depends linearly on bulk drop concentration C_0, as predicted if $C_e \ll C_0$. This is seen by replotting the data of Fig. 3 after normalization by the drop composition, noting that for dilute Cu–Cr alloys used here, the Cr molar fraction x is simply proportional to its concentration; hence, $C_0 - C_e$ is proportional to $\Delta x = \bar{x}_0 - x_e$. The equilibrium value, x_e, is calculated from thermodynamic data [13] to be 7×10^{-4}, while the average bulk drop concentration $\bar{x}_0$ is estimated as $\bar{x}_0 = (x_{t_1} + x_{f,cal})/2$ (see Table 1). After normalization by Δx, the curves for three drops having nearly equal mass (of 100 mg) but different Cr content belong, nearly, to the same curve [Fig. 3(c)]. This substantiates the dependence of spreading rate on concentration expected from the nature of the problem at hand (diffusion equations being linear in concentration), and which is contained in equation (1).

Experimental results disagree, however, with model predictions in that the measured velocity is not directly proportional to θ. Instead, although the relationship between dR/dt and θ is approximately linear for $\theta < 90^\circ$, the intercept with the θ-axis (i.e. the point where dR/dt becomes zero) is not at the origin (i.e. at $\theta = 0$), but rather near the equilibrium contact angle θ_e of about 41° (see Figs 2, 3, 7 and 8). For $\theta > 90^\circ$, there is, additionally, a positive deviation from the linear relationship that seems to hold at lower contact angles. As a consequence, $R(t)$ curves clearly cannot be described at small θ as functions of the form $R^n - R_0^n = k(t - t_0)$ where k, t_0 and n are constants.

The sharp deviation from linearity observed at $\theta \geq 90^\circ$ can be explained by evaporation of solute from the drop surface during the spreading process. The existence of such evaporation is provided by drop mass losses indicated above. Hence, when the droplet-free surface forms an acute angle through the vapor phase with the substrate, evaporation/condensation can provide a parallel transport path for chromium from the drop to the triple line. This should accelerate dR/dt to an extent that increases as θ increases beyond 90°; this is indeed observed.

The discrepancy with the model at $\theta < 90^\circ$ is somewhat more difficult to explain. Its most likely source is, we believe, in the assumption made in the calculation of Ref. [12] that, during spreading, reaction takes place only at the triple line and not along the liquid–solid interface behind the triple line. Such reaction can influence diffusion-limited spreading kinetics in two ways: (i) by causing a gradual lowering of the bulk drop concentration C_0 with time; and (ii) by diverting solute flux lines in the wedge near the triple line away from the triple line, towards the liquid–solid interface.

The first effect, namely the influence on spreading kinetics of a time-dependent decrease in bulk drop concentration C_0 caused by interfacial reactions is analyzed in Appendix A. It is found that variations in C_0 caused during spreading by carbide formation (chromium depletion during spreading of the transferred drops is nearly entirely due to interfacial reaction) do indeed alter somewhat the predicted relationship between drop spreading velocity dR/dt and contact angle θ; however, the effect is limited and cannot explain alone the observed discrepancy between data and equation (1).

We therefore examine whether the second effect, namely diversion of solute diffusion lines from the triple line due to continued reaction behind the triple line, could cause a shift in the (linear) plot of dR/dt vs θ, such that it meets the θ-axis at a finite value of θ (Figs 2, 3, 7 and 8). To this end, we use the conclusion from Ref. [12] that diffusion to the triple line can be analyzed essentially as a steady-state diffusion problem, dependent on time only through its dependence on θ. We thus solve, while maintaining other assumptions and boundary conditions of Ref. [12], the opposite extreme case, for which there is rapid reaction along all contact areas between solid and liquid, i.e. both at, and behind, the triple line.

This problem is stated in graphical form in Fig. 9: we solve for steady-state diffusion from bulk liquid at C_0 through a cylindrical wedge, to (i) the triple line, represented as in Ref. [12] by a small arc of cylinder of radius a and angle θ, and also (ii) to the liquid–solid interface, both surfaces being at the equilibrium concentration C_e. That the equilibrium

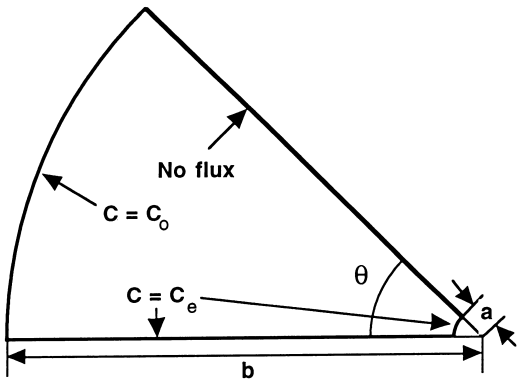

Fig. 9. Schematic description of simplified geometry and boundary conditions for reactive wetting with continued reaction everywhere along the liquid–solid interface behind the triple line.

concentration is present everywhere along the liquid–solid interface supposes very strong and continuous chemical interaction between solid and liquid, free of hindrance by solid already formed. As such, this represents an extreme case of chemical interaction along the interface, opposite to that of no interaction at all behind the triple line which was treated in Ref. [12].

This steady-state diffusion problem is solved in Appendix B, to show that the triple line velocity is now given by:

$$\frac{\mathrm{d}R}{\mathrm{d}t} = \frac{4(C_0 - C_\mathrm{e})D}{\pi e n_\mathrm{v}} \times \sum_{n=0}^{\infty} \frac{1}{(2n+1)} \frac{1}{\sinh\left(\dfrac{(2n+1)\pi}{2\theta} \ln\left(\dfrac{b}{a}\right)\right)} \quad (2)$$

At values of θ sufficiently large so that $\sin h(x) \approx x$ for the first terms of the series on the right-hand side of equation (2), the series which it contains approaches $\pi\theta[4\ln(b/a)]^{-1}$ [14]. Thus, for large values of θ, equation (2) tends towards the expression derived for a steady-state solute profile with no diffusion to the liquid–solid interface behind the triple line:

$$\frac{\mathrm{d}R}{\mathrm{d}t} = \frac{(C_0 - C_\mathrm{e})D\theta}{e n_\mathrm{v} \ln\left(\dfrac{b}{a}\right)} \quad (3)$$

A plot of

$$Y_{(X)} = \sum_{n=0}^{\infty} \frac{1}{(2n+1)} \frac{1}{\sinh\left(\dfrac{(2n+1)}{X}\right)} \quad (4)$$

is given in Fig. 10. It is seen that this function does, indeed, reproduce the shape of experimentally observed curves of $\mathrm{d}R/\mathrm{d}t$ vs θ: the curve is essentially straight for larger θ, and its prolongation intercepts the horizontal axis for a finite positive value of X, on the order of 0.25. This suggests that, from a physical standpoint, solute diffusion to an isoconcentrate liquid–solid interface essentially substracts a finite and constant angle θ_d from that through which diffusion can transport solute from the drop bulk to the triple line. Thus, essentially, continued reaction behind the triple line causes a diversion of solute flux lines away from the triple line towards the drop–substrate interface within a wedge of relatively constant angle θ_d, effectively replacing θ by $(\theta - \theta_\mathrm{d})$ in equation (1).

This would lend credence to the interpretation offered for the observed discrepancy between equation (1) and experimental data in this work, namely that it is diffusion of solute to the liquid–solid interface behind the triple line that causes a shift in the (still) linear relation between $\mathrm{d}R/\mathrm{d}t$ and θ. We note, however, that the extreme assumption that $C = C_\mathrm{e}$ everywhere behind the triple line results in a value for θ_d that is unrealistically large: $X = 0.25$ corresponds, if we take $\ln(b/a) \approx 12$ as suggested by the analysis in Ref. [12] for diffusion to the triple line only, to $\theta_\mathrm{d} \approx 3\pi/2$. This value, despite being of the right order of magnitude, is clearly too large; however, the calculation does provide an indication that the effect of continued reaction along the interface behind the triple line is to prevent solute within a constant liquid wedge from reaching the triple line.

If we therefore assume that solute diffusion to the liquid–solid interface essentially results in the presence of a constant "dead angle" θ_d within which solute diffusion from the bulk is diverted to the interface before reaching the triple line, as depicted in Fig. 11(a), θ must simply be replaced by $(\theta - \theta_\mathrm{d})$ in equation (1) [Fig. 11(b); we note that proximity of θ_d with the equilibrium contact angle on the reaction product, $\theta_\mathrm{e} = 41^\circ$ is fortuitous according to this interpretation]. We can then compare the observed slope of $\mathrm{d}R/\mathrm{d}t$ vs θ, which is on the order

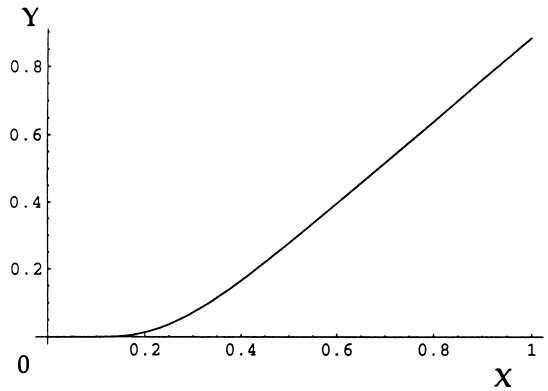

Fig. 10. Plot of $Y_{(X)}$ defined by equation (4), giving the dimensionless shape of triple line velocity for diffusion-limited reactive wetting with continued reaction everywhere along the liquid–solid interface behind the triple line, as described by Fig. 9.

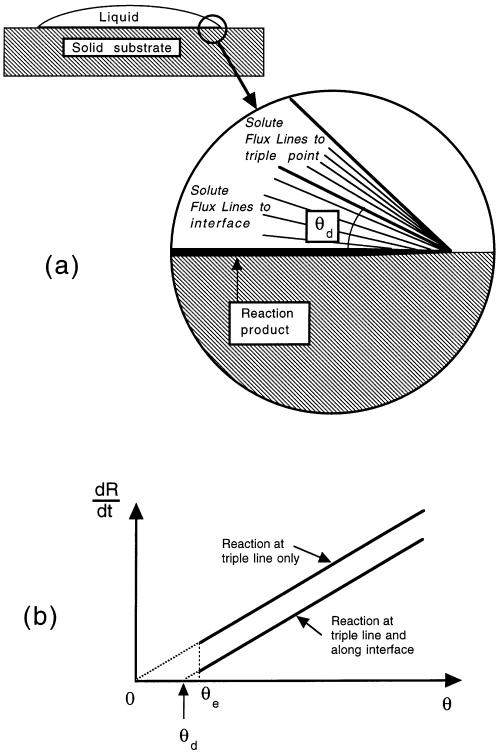

Fig. 11. Schematic description of the expected influence of continued reaction behind the triple line on the rate of diffusion-controlled spreading: (a) continued reaction behind the triple line diverts solute flux lines within an angle θ_d away from the triple line; (b) provided θ_d varies little with the contact angle θ, spreading kinetics are predicted by equation (1) after replacement of θ by $(\theta - \theta_d)$. In both cases, spreading stops when the contact angle θ equals θ_e, the equilibrium contact angle of the liquid on the reaction product.

of 3×10^{-3} cm/s with $x_{Cr} = 1$ at.% from data in Fig. 2, with the value that is predicted by equation (1). Estimating values for relevant parameters as $D \approx 4 \times 10^{-5}$ cm^2/s (typical of transition metals in copper at 1373 K [15]), average molar volume of atoms in the liquid equalling $\rho_{Cu}/MW_{Cu} = 8/63.5 = 0.126$ mol/cm^3, and $n_v \approx 2 \times 6.63/180 = 0.074$ mol/cm^3 (based on values for Cr_3C_2 for lack of data for Cr_7C_3) [15, 16], we find that the thickness, e, of the reaction product layer formed during spreading at the triple line (and not the final carbide thickness) must be:

$$e = \left(\frac{2FDC_0}{n_v}\right)\left[\frac{(\theta - \theta_d)}{\left(\frac{dR}{dt}\right)}\right] \approx 0.2\ \mu m$$

This is a physically plausible value for the reaction product thickness required to form, by reaction at and/or ahead of the triple line, a continuous carbide layer over which the drop can spread. Indeed, the reaction layer is found to be composed of grains below one micron in size [8], the initial coalescence of which into a continuous layer could indeed create a layer about 0.2 μm in initial thickness. Furthermore, this value of e is lower than the one to five micrometers of the final observed reaction layer thickness, which reinforces the suggestion that there is significant reaction between drop and substrate behind the triple line, after spreading of the liquid over the initially formed carbide. The calculated value of e is thus consistent with the interpretation that deviations in triple line spreading kinetics from predictions of Ref. [12] are due to deviation of solute diffusion flux lines to the liquid–solid interface behind the triple line. However, more work, both experimental and theoretical, is needed for this interpretation of the data to rest on firm ground.

5. CONCLUSION

Transferred sessile drop experiments conducted with Cu–Cr alloys on vitreous carbon substrates indicate that wetting is improved by drop–substrate chemical interaction which leads to the formation of a layer of the compound Cr_7C_3 of thickness 1–5 μm. As a consequence of interaction, the final contact angle decreases from about 137° for pure Cu to about 40° for Cu alloyed with Cr.

Analysis of the spreading kinetics indicates that the rate of spreading is limited by Cr diffusion to the triple line. In accordance with the predictions of a previously published analysis of spreading limited by solute diffusion from the bulk drop to the triple line, the observed rates of spreading are indeed:

1. for a given alloy, a function of the instantaneous contact angle θ only;
2. linearly dependent on θ within experimental uncertainty for $\theta < 90^\circ$;
3. proportional to the drop solute content; and
4. independent of drop mass.

Discrepancies with the predictions of the analysis are observed, however, in that (i) at angles higher than 90°, there is an upward deviation in the spreading rate from the linear relation observed at lower angles, and (ii) the intercept of the line of dR/dt vs θ with the θ-axis is not at the origin ($\theta = 0$), but near $\theta = 40^\circ$. The former deviation is attributed to short-circuit solute transport in front of the triple line by evaporation from the drop surface. The second discrepancy is explained as resulting from continued drop–substrate chemical reaction behind the triple line, which reduces the solute flux reaching the triple line from the drop bulk, and causes a time dependence in the bulk drop solute concentration.

Acknowledgements—This study was performed during a post-doctoral year of R. Voitovitch in Grenoble thanks to a grant from the French Ministry of Research and Education. A. Mortensen gratefully acknowledges partial support for this work from the National Science Foundation, grant number MSS-92-01843, and the French Ministry of Research and Education for a Bourse de Haut Niveau supporting sabbatical leave in France.

REFERENCES

1. Espié, L., Drevet, B. and Eustathopoulos, N., *Metall. Mater. Trans.*, 1994, **25A**, 599.
2. Kritsalis, P., Drevet, B., Valignat, N. and Eustathopoulos, N., *Scripta metall. mater.*, 1994, **30**, 1127.
3. Eustathopoulos, N. and Drevet, B., *J. Physique*, 1994, **4**, 1865.
4. Naidich, Y., Zabuyga, B. and Perevertailo, V., *Adgeziya Raspi. Pajka Mater.*, 1992, **27**, 23.
5. Landry, K. and Eustathopoulos, N., *Acta mater.*, 1996, **44**, 3923.
6. Landry, K., Rado, C. and Eustathopoulos, N., *Metall. Trans.*, 1996, **27A**, 3181.
7. Drevet, B., Landry, K., Vikner, P. and Eustathopoulos, N., *Scripta mater.*, 1996, **35**, 1265.
8. Landry, K., Rado, C., Voitovitch, R. and Eustathopoulos, N., *Acta mater.*, 1997, **45**, 3079.
9. Mortimer, D.A. and Nicholas, M., *J. Mater. Sci.*, 1973, **8**, 640.
10. Devincent, S.M. and Michal, G.M., *Metall. Trans.*, 1993, **24A**, 53.
11. Kritsalis, P., Li, J.G., Coudurier, L. and Eustathopoulos, N., *J. Mater. Sci. Lett.*, 1990, **9**, 1332.
12. Mortensen, A., Drevet, B. and Eustathopoulos, N., *Scripta mater.*, 1997, **36**, 645.
13. Kubaschewski, O., Alcock, C.B. and Spencer, R.J., *Metallurgical Thermochemistry*, 6th edn. Pergamon Press, Oxford, 1993.
14. Tuma, J.J., *Engineering Mathematics Handbook*. McGraw-Hill, New York, 1979, p. 99.
15. Weast, R.C., Lide, D.R., Astle, M.J. and Beyer, W.H., ed., *CRC Handbook of Chemistry and Physics*, 70th edn. CRC Press, Boca Raton, FL, 1990, pp. B-85 and F-52.
16. Brandes, E.A., ed., *Smithells Metals Reference Book*, 6th edn. Butterworths, London, 1983, pp. 2-27 and 14-6.
17. Carslaw, H.S. and Jaeger, J.C., *Conduction of Heat in Solids*, 2nd edn. Clarendon Press, Oxford, 1959, pp. 166–167 and 431–434.

APPENDIX A

Influence of bulk drop solute depletion on diffusion-limited drop spreading kinetics

If the bulk drop concentration C_0 decreases with time due to formation of a reaction layer of constant thickness along the liquid–solid interface, C_0 will vary with drop contact area radius R according to:

$$C_0 = C_{0,\,\text{initial}} - \left(C_{0,\,\text{initial}} - C_{0,\,\text{final}}\right)\frac{R^2}{R_{\text{final}}^2} \tag{A.1}$$

where $C_{0,\,\text{initial}}$ and $C_{0,\,\text{final}}$ are the bulk drop solute concentrations upon initial contact of the drop with the substrate, and at final equilibrium of the drop on the reaction product, respectively, and R_{final} is the drop contact area radius at the end of spreading (i.e. at equilibrium). Given the small size of the drops, their shape approximates that of a hemispherical cap. Hence, the drop–substrate contact area radius R and the contact angle e are linked by:

$$R = \left(\frac{V}{\pi}\right)^{1/3}\left(\frac{3\sin(\theta)}{2 - 3\cos(\theta) + \cos^2(\theta)}\right)^{1/3} \tag{A.2}$$

By insertion of equations (A.1) and (A.2) into equation (1), one obtains the following modified equation for the drop spreading rate, dR/dt:

$$\frac{dR}{dt} = \frac{2DF_{(t)}}{en_{\text{v}}}\,\theta\left[C_{0,\,\text{initial}} - C_{\text{e}} - \left(C_{0,\,\text{initial}} - C_{0,\,\text{final}}\right)\left(\frac{(\sin(\theta))\left(2 - 3\cos(\theta_{\text{f}}) + \cos^2(\theta_{\text{f}})\right)}{\left(\sin(\theta_{\text{f}})\right)\left(2 - 3\cos(\theta) + \cos^2(\theta)\right)}\right)^{2/3}\right] \tag{A.3}$$

where θ_{f} is the final (equilibrium) contact angle of the drop on the reaction product. The resulting curve is traced in Fig. 1A for values typical of the present experiments: $C_{0,\,\text{initial}}$ and $C_{0,\,\text{final}}$ corresponding, respectively, to $x_{\text{in}} = 0.0087$ and $x_{\text{f,cal}} = 0.0051$ (see Table 1), $n_{\text{v,B}} = 0.074\ \text{mol/cm}^3$, $D = 4 \times 10^{-5}\ \text{cm}^2/\text{s}$, $F_{(t)} = 0.04$, and $e = 0.2\ \mu\text{m}$ (see Discussion, Section 4). Comparison of this curve with that predicted by equation (1) with C_0 constant and equal to the average of

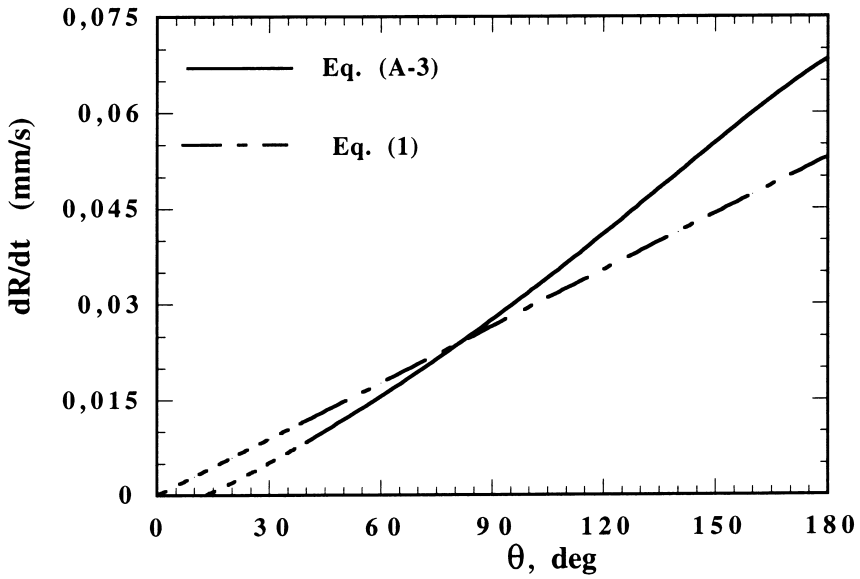

Fig. 1A. Comparison of predicted triple line velocity dR/dt vs contact angle θ from equations (1) and (A.3), showing that a straight-line extrapolation of the latter curve will intercept the θ-axis at a finite value of θ, near 20° for conditions typical of the present experiments.

$C_{0,\text{ initial}}$ and $C_{0,\text{ final}}$ (corresponding to $\bar{x}_0 = 0.0069$) shows that solute depletion causes an apparent tilting of the curve giving dR/dt vs θ for $\theta > 41°$. This effect can thus account in part for the apparent θ-axis intercept of the plot of (dR/dt) vs θ not being at the origin; however, its influence is too small to account for the experimentally observed curve shapes. We note that this effect also is insufficient to account for the deviations observed at $\theta > 90°$.

APPENDIX B

Calculation of diffusion-limited drop spreading with continued chemical reaction along the liquid–solid interface

We seek a solution to the problem defined by

$$0 \le \alpha \le \theta,\ a \le r \le b,\ \Delta C = 0 \tag{B.1}$$

where Δ denotes the Laplacian operator, α is used here to denote the angular cylindrical coordinate (so as to avoid confusion with θ, which denotes the drop contact angle), subject to boundary conditions:

$$r = a,\ 0 \le \alpha \le \theta,\ C = C_e \tag{B.2}$$

$$r = b,\ 0 \le \alpha \le \theta,\ C = C_0 \tag{B.3}$$

$$\alpha = 0,\ a \le r \le b,\ C = C_e \tag{B.4}$$

$$\alpha = \theta,\ a \le r \le b,\ \partial C/\partial \alpha = 0 \tag{B.5}$$

With $b = a \exp(1/[2F_{(t)}]) \approx 3 \times 10^5 a$,† and the boundary condition given by equation (B.4) replaced by a no-flux condition such as equation (B.5), this problem is similar to that solved in equation (15) of Ref. [12].

By symmetry, the solution to this problem is similar to that defined by boundary conditions:

$$r = a,\ 0 \le \alpha \le 2\theta\ C = C_e \tag{B.6}$$

$$r = b,\ 0 \le \alpha \le 2\theta\ C = C_0 \tag{B.7}$$

$$\alpha = 0 \text{ and } \alpha = 2\theta,\ a \le r \le b,\ C = C_e \tag{B.8}$$

This diffusion problem is solved using the conjugate function $\xi + i\eta$ defined by Ref. [17],

†There is, unfortunately, a typographical error in Ref. [12], where the factor 2 has been omitted.

$$\xi = \frac{\pi}{\theta}\alpha, \text{ and } \eta = \frac{\pi}{\theta}\ln\left(\frac{b}{r}\right) \tag{B.9}$$

such that we now have to solve the rectangular problem

$$0 \le \xi \le 2\pi,\ 0 \le \eta = \frac{\pi}{\theta}\ln\left(\frac{b}{a}\right),\ \Delta C = 0 \tag{B.10}$$

with boundary conditions:

$$0 \le \xi \le 2\pi,\ \eta = \frac{\pi}{\theta}\ln\left(\frac{b}{a}\right),\ C = C_e \tag{B.11}$$

$$0 \le \xi \le 2\pi,\ \eta = 0,\ C = C_0 \tag{B.12}$$

$$\xi = 0 \text{ and } \xi = 2\pi,\ 0 \le \eta = \frac{\pi}{\theta}\ln\left(\frac{b}{a}\right),\ C = C_e \tag{B.13}$$

The solution to the rectangular problem is [17]

$$C = C_e + \frac{4(C_0 - C_e)}{\pi}\sum_{n=0}^{\infty}\frac{1}{(2n+1)}\sin\left(\frac{(2n+1)\pi\xi}{2\pi}\right)\frac{\sinh\left(\dfrac{(2n+1)\pi\left(\frac{\pi}{\theta}\ln\left(\frac{b}{a}\right)-\eta\right)}{2\pi}\right)}{\sinh\left(\dfrac{(2n+1)\pi}{2\theta}\ln\left(\frac{b}{a}\right)\right)} \tag{B.14}$$

or, after transformation back to coordinates r and θ:

$$C = C_e + \frac{4(C_0 - C_e)}{\pi}\sum_{n=0}^{\infty}\frac{1}{(2n+1)}\sin\left(\frac{(2n+1)\pi\theta}{2\theta}\right)\frac{\sinh\left(\dfrac{(2n+1)\pi}{2\theta}\ln\left(\frac{r}{a}\right)\right)}{\sinh\left(\dfrac{(2n+1)\pi}{2\theta}\ln\left(\frac{b}{a}\right)\right)} \tag{B.15}$$

The triple line velocity is then given by calculating the total flux of solute reaching the triple line

$$\frac{dR}{dt} = \frac{Da}{en_v}\int_0^{\theta}\left(\frac{\partial C}{\partial r}\right)_{r=a}d\theta \tag{B.16}$$

yielding

$$\frac{dR}{dt} = \frac{4(C_0 - C_e)D}{\pi e n_v}\int_0^{\theta}\sum_{n=0}^{\infty}\frac{\pi}{2\theta}\sin\left(\frac{(2n+1)\pi\alpha}{2\theta}\right)\frac{d\alpha}{\sinh\left(\dfrac{(2n+1)\pi}{2\theta}\ln\left(\frac{b}{a}\right)\right)} \tag{B.17}$$

or, after integration and simplification, the expression given in equation (2).